Microresonant accelerometer composed of silicon substrate and quartz double-ended tuning fork with temperature isolator

Cun Li, Yulong Zhao, Rongjun Cheng, Zhongliang Yu

State Key Laboratory for Manufacturing System Engineering, Xi'an Jiaotong University, Xi'an, Shannxi 710049, People's Republic of China
E-mail: zhaoyulong@mail.xjtu.edu.cn

Published in Micro & Nano Letters; Received on 15th May 2014; Revised on 17th August 2014; Accepted on 18th August 2014

A microresonant accelerometer which consists of silicon substrate and a quartz double-ended tuning fork (DETF) is described. A temperature isolator structure on the silicon substrate is designed to decrease the influence of thermal stress on the DETF's tines. Two stiff ends of the quartz DETF are mounted on the proof mass and temperature isolator, respectively. When acceleration is applied, the proof mass will move, inducing the variation of axial stress on the DETF's tines. The resonance frequency of the DETF's tines will change corresponding to the stress, so acceleration can be measured. The DETF is excited by the inherent piezoelectric property of quartz based on the anti-phase in-plane bending model. Both the silicon substrate and the DETF are fabricated by micromachining. The sensor is analysed by finite-element simulation. According to the simulation, the temperature isolator decreases thermal stress by 30.2%. Experimental results show that the resonance frequency of the sensor is 35.2563 kHz and the sensitivity is 8.55 Hz/*g*, which is in good agreement with analytical calculation.

1. Introduction: Resonant accelerometers, utilising the shifting frequency corresponding to acceleration, have been adopted to replace the analogue accelerometers for inertial and flight control applications. The resonant sensor has attracted a great deal of attention owing to its high precision and wide dynamic range. Moreover, the digital output makes it easy to integrate into digital systems and improve the accuracy.

Many research works have been conducted on the microresonant accelerometer since it was reported by Albert in 1982 [1]. Silicon is widely used for microsensors because of its mature manufacturing process and good material property. Many different configurations of silicon resonant sensors have been designed and implemented [2, 3]. As the silicon material does not present the piezoelectric property, the excitation of vibration for resonant elements should be achieved by other materials or methods. The excitation methods mainly include electrostatic excitation [4], piezoelectric excitation [5], electrothermal excitation [6] and electromagnetic excitation [7], and the sensing element is typically accomplished by means of piezoresistive, capacitive or piezoelectric methods. The external excitation methods complicate the sensor structure and the fabrication process, and the quality is relatively low. Quartz has been widely used as a resonator material for a long time in microsensors, because of its good material properties such as high-quality factor, low aging rates and inherent piezoelectric effect [1]. The quartz resonant accelerometers can be fabricated in two ways. One is by attaching the quartz double-ended tuning fork (DETF) to a metal substrate with proof mass for sensing acceleration [8, 9]. However, the metal substrate makes it quite difficult to achieve massive production. The other one is fabricated from monolithic quartz [10, 11]. Owing to the complicated structure and the difficult fabrication of the quartz material, only one vibration beam can be fabricated.

The uniqueness in our research is that we combined both the quartz and silicon materials for developing a resonant accelerometer. The quartz DETF working as the sensing element is mounted on the silicon substrate, so the sensor can be excited easily by the inherent piezoelectric effect of quartz. The advantage of using silicon substrate is that it can be fabricated massively and precisely. To reduce the influence of temperature induced by the thermal expansion difference between the quartz and silicon materials, a temperature isolator structure is designed.

2. Sensor operating principle and design: The resonant sensor is mainly made up of silicon substrate and the quartz DETF. This Section concerns the description of its working principle, and the design of the silicon substrate including the temperature isolator structure and the quartz DETF.

2.1. Sensor description and operating principle: A schematic diagram of the accelerometer structure is shown in Fig. 1. The structure consists of a movable proof mass suspended by two parallel flexure hinges and the DETF formed by two microbeams vibrating in an anti-phase in-plane bending model. Two stiff ends of the quartz DETF are mounted on the proof mass and temperature isolator structure, respectively. The applied acceleration moves the proof mass in the positive/negative sensing direction, so the tines of the DETF undergo tensile/compressive axial stress which shifts the vibrational frequency. The change of internal axial stress in the resonator converts the measured quantity (acceleration) to the DETF's resonance frequency shift. The resonant frequency of the microbeam is related to the axial stress and, in turn, to the acceleration along the sensing direction.

The sensor is designed to measure 100 *g*. A Pyrex glass is bonded under the silicon frame, and there is a protective clearance

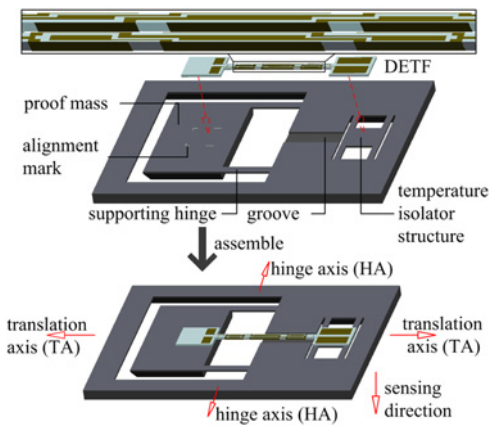

Figure 1 *Diagrammatic sketch of the resonant accelerometer*

doi: 10.1049/mnl.2014.0265

between the proof mass and the Pyrex glass to protect the sensor from being damaged under overload. Moreover, the adopted sensor dimensions can also provide a conservatively high range with a maximum admissible acceleration of 1000 g.

The level of thermal expansion mismatch between the single-crystal silicon and quartz is very important for determining temperature sensitivity. Owing to the different coefficients of thermal expansion between these two materials, the thermal stress in the DETF's vibration beam will change corresponding to the temperature. On the silicon substrate, a temperature isolator is designed to decrease the temperature effect as presented in Fig. 1. Two points must be ensured: (i) it is relatively compliant for DETF movement parallel to transducer axis (TA); (ii) it is relatively non-compliant for isolator rotation about the hinge axis (HA). When temperature changes, the flexibility parallel to the TA direction is able to reduce the thermal stress to a certain extent. Non-compliance with isolator rotation about the HA makes the isolator influence sensor sensitivity as minimal as possible.

2.2. Design of the DETF: The DETF is fabricated from Z-cut quartz crystal wafer. The tine length is along the Y crystal axis, and the width is in the X-direction. For exciting the anti-phase in-plane vibration mode, electrodes are deposited on the top, bottom and on the two sidewalls of the vibration tines. The electrical polarity changes two times at the nodal points where the stress is zero or minimum. Figs. 2*a*–*c* illustrate the electrode arrangement, the electric field in one tine and the flexure vibration mode, respectively. The electric field, which will contribute to the piezoelectric effect, is mainly from the X-direction. According to the piezoelectric effect of Z-cut quartz crystal, the stress caused by the X-direction electric field is along the tine length direction, and bends the tine in the fundamental flexure mode, as shown in Fig. 2*c*. This kind of vibration mode has a high-quality factor because of the self-balance of the inner stress and the torque on the combining ends of the tines.

2.3. Design of the silicon substrate: For flexural vibration of a clamped–clamped beam, the motion of the vibrating beam can be modelled by the Euler-Bernoulli equation. When an axial stress σ is induced in the beam, the resonant frequency f_1 for the fundamental vibration mode can be expressed as [12, 13]

$$f_1(\sigma) = \frac{4.73^2}{2\pi l^2}\sqrt{\frac{EI}{\rho A}}\sqrt{1 + 0.2949\frac{\sigma l^2}{Ew^2}} \quad (1)$$

where E represents the Young's modulus, $I = hw^3/12$ is the moment of inertia where h and w are the thickness and width, l is the beam length, ρ is the beam density, $A = hw$ and σ is the axial stress.

By inserting into (1) the dimensions of the DETF microbeam ($h = 100$ μm, $w = 90$ μm, $l = 3.74$ mm) and the material parameters of quartz ($E = 9 \times 10^{10}$ N/m^2, $\rho = 2.65 \times 10^3$ kg/m^3), the resonant frequency f_1 in the unloaded case, that is, for $\sigma = 0$, can be calculated, resulting in $f_1 = 38.535$ kHz. The finite-element (FE) simulation frequency is $f_1 = 34.581$ kHz.

The FE thermal stress analysis method was used to calculate the thermal stress for predicting the effect of temperature when the temperature changed from 25 to 50°C. The dimensions of proof mass and the hinge beams are shown in Fig. 3. The uniform thickness of the isolator and hinge beam can simplify the manufacture process. For the given dimensions of proof mass and hinge beams, the beam size of the isolator becomes the major factor that affects thermal stress.

The thermal stress in the vibration beam with different isolator beam dimensions was simulated and is shown in Fig. 4 when the temperature changes from 25 to 50°C. In Fig. 4, the listed stress is along the central axis of the DETF's tine. In the simulation, the dimensions of the proof mass and hinge beams are kept constant as shown in Fig. 3. The thickness of the isolator is designed to be equal to the thickness of the hinges for simplifying the manufacture process. For the condition of a beam width larger than 300 μm, the

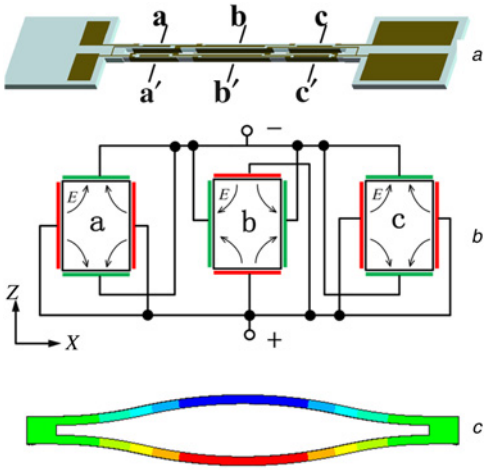

Figure 2 *Design of the quartz DETF*
a Structure of the quartz DETF and the electrodes distribution
b Diagrammatic sketch of the electrode connection and electrical polarity in one single tine from a–a′, b–b′, and c–c′ cross-sections
c Anti-phase in-plane bending model
The Figure was the result of piezoelectricity simulation based on the structure and electrode distribution shown in (Fig. 1*a*)

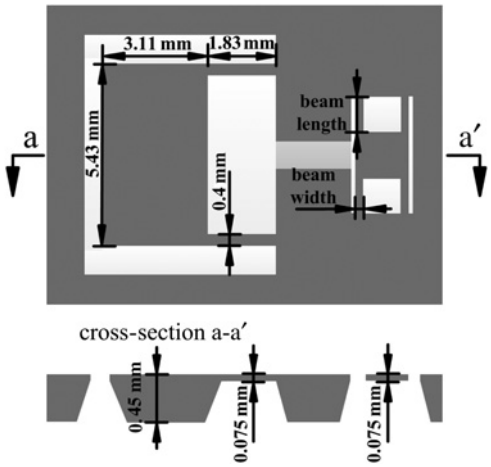

Figure 3 *Dimensions of proof mass and suspension beams*

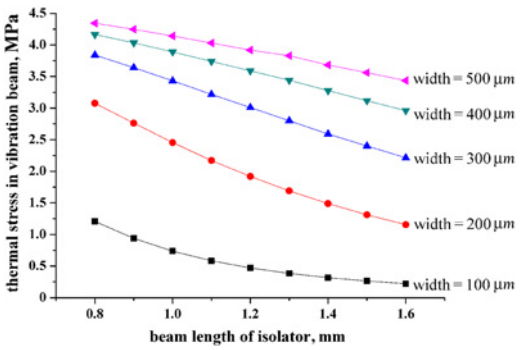

Figure 4 *Variation of thermal stress in vibration beam with different isolator beam lengths and widths*

effectiveness on thermal stress for a smaller isolator size is becoming much weaker. If thermal stress is the only factor taken into consideration, a higher ratio of length/width should be the best choice, which means higher flexibility along the DETF's tine direction and lower thermal stress in the tines. A more flexible isolator also decreases acceleration sensitivity, so the finally designed isolator beam length is 1 mm and the width is 0.25 mm.

A comparison of thermal stress with and without the use of an isolator for the same proof mass and hinge beam dimensions is presented in Fig. 5. It can be seen that the thermal stress decreases by nearly 30.2% from 4.3 to 3.0 MPa. The theoretical analysis proves the effectiveness of the isolator.

The sensitivity for the proposed sensor size can be calculated using the following method: (i) the axial stress induced by acceleration was determined by FE simulation; (ii) the stress is substituted into (1) to calculate the frequency shift. For the proposed sensor size, the simulated axial stress parallel to the beam length is 8.511 MPa when 100 g acceleration is applied. Substituting this into (1), the frequency shift can be calculated and the result is 917 Hz, that is to say, the sensitivity of the proposed accelerometer is 9.17 Hz/g. Then, we analysed the influence of the isolator on the acceleration sensitivity. For the sensor size in Fig. 3, the acceleration sensitivity decreases from 14.18 to 9.17 Hz/g. The isolator structure also decreases the acceleration sensitivity; however, the final sensitivity 9.17 Hz/g is also enough for application, and this sensitivity can be improved further by reducing the dimensions of the suspension beam and by enlarging proof mass.

3. Realisations: The silicon substrate was fabricated by bulk micromachining technology on a 4-inch (100) wafer, the thickness of which is 450 µm. The silicon wafer was first etched 375 µm by an anisotropic KOH etchant on the backside of the silicon wafer. Then, an inductively coupled plasma etching process followed to etch 75 µm on the frontside for releasing the structure. The DETF was produced using photolithographic, chemical etching and metal deposit techniques.

The main fabrication process of the DETF is shown in Fig. 6, which mainly includes the following six steps. (i) Clean the quartz wafer, and deposit the Cr/Au layer. Pattern the photoresist by photolithographic techniques. (ii) Etch the Cr/Au layer. The Cr layer is etched by the mixed solution of ceric ammonium nitrate and acetic acid. The etchant for Au etching is I_2 and KI solution. (iii) Etch quartz using the fluoride-based solution (40% HF:40% NH_4F = 1:1). (iv) Fabricate the electrodes on the planar surface using photolithographic technology and Cr/Au wet etching method. (v) Deposit the Cr/Au layer on the left sidewall of the tuning fork. A hard mask is used in this step. (vi) Deposit the Cr/Au layer on the right sidewall. The finished DETF and the

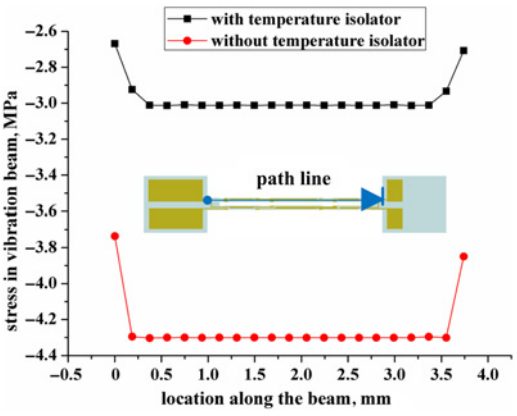

Figure 5 *Comparison of thermal stress in DETF with and without temperature isolator structure*

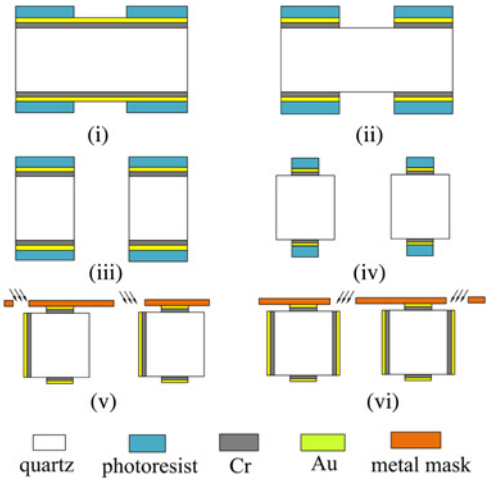

Figure 6 *Main fabrication process of DETF*

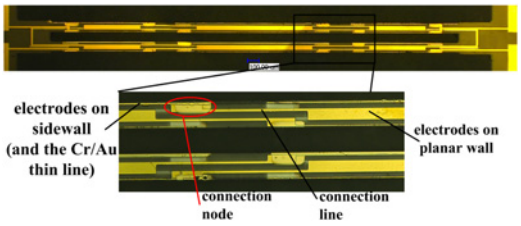

Figure 7 *Photograph of the finished DETF*

sidewall profile of the tine after releasing the DETF structure are shown in Figs. 7 and 8, respectively. The connection node presented in Fig. 7 is used to connect the electrodes on the planar and sidewalls. For connection reliability, a very thin Cr/Au line is designed on the edge of the planar surface.

Then, the silicon substrate and the DETF were bonded together by epoxy glue, and the sensor was packaged simply for characterisation as shown in Fig. 9. The epoxy glue used for bonding the silicon substrate and quartz DETF was specially developed to make sure that its coefficient of thermal expansion is very close to that of the quartz crystal. We mixed the powder of quartz crystal into the glue to achieve the desired thermal expansion coefficient and let it be close to that of the quartz. In the whole bonding process, external force is applied on the DETF to decrease the thickness of the glue, which decreases the influence of the glue on sensor's temperature property.

The resonance accelerometer was excited through a self-excited circuit which was connected to the electrodes deposited on the

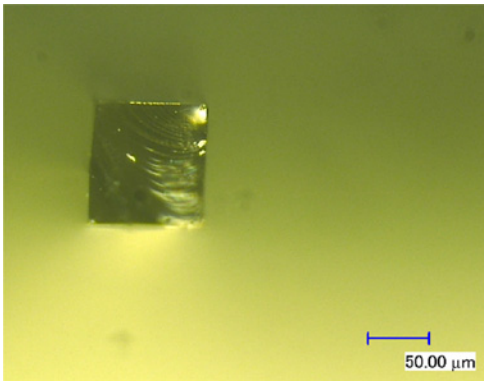

Figure 8 *Sidewall profile of the tine after releasing the DETF structure*

doi: 10.1049/mnl.2014.0265

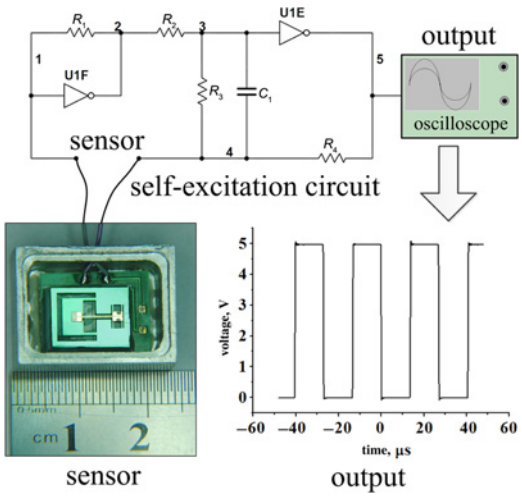

Figure 9 *Simply packaged sensor, self-excitation circuit and output square wave*

DETF's tines. The self-excited circuit mainly is composed of two phase inverters as shown in Fig. 9. Resistors R_1, R_2, R_3 and R_4 ensure that both the inverters functioned at the linear amplification condition. Capacitance C_1 was used to eliminate high-frequency harmonics. This circuit offers advantages such as a simple configuration, stable performance, as well as a wide adjustment range for the parameters of electronic components. With the circuit parameters $R_1 = 900$ kΩ, $R_2 = 2.56$ kΩ, $R_3 = 100$ kΩ, $R_4 = 100$ kΩ, $C_1 = 10$ pF, the circuit could oscillate stably, and the output square wave was recorded by an oscilloscope. The packaged sensor, self-excitation circuit and the output square wave are presented in Fig. 9.

4. Experiment and results: The characteristics of the packaged resonant accelerometer were evaluated, including sensitivity, nonlinearity, hysteresis, output fluctuation and temperature drift. In the whole experiment process, a frequency calculator (Fluke 8845A) was used to record the resonant frequency of the sensor.

Static sensitivity measurements were performed by mounting the sensor on a precise dividing head, as shown in Fig. 10*a*. The dividing head rotates from 0 to 360° in the earth's gravitational field, and the acceleration applied on the sensor's sensing direction changes from 1 to −1 *g*, then finally back to 1 *g* as shown in Fig. 10*b*. The acceleration along the sensor's sensing direction can be calculated as

$$a = g\cos(\theta) \tag{2}$$

where g is the gravitational acceleration and θ is the rotation angle of the dividing head.

The results of the tumbling experiment are shown in Fig. 11. The output of the sensor changes from 35.2653 to 35.2482 kHz when

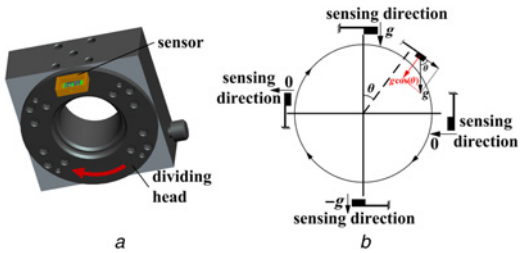

Figure 10 *Schematic diagram of tumbling experiment*
a Structure of the dividing head and the sensor assembly
b Changing process of acceleration along the sensor's sensing direction

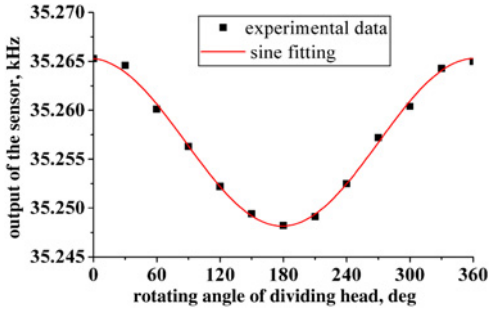

Figure 11 *Results of tumbling experiment*

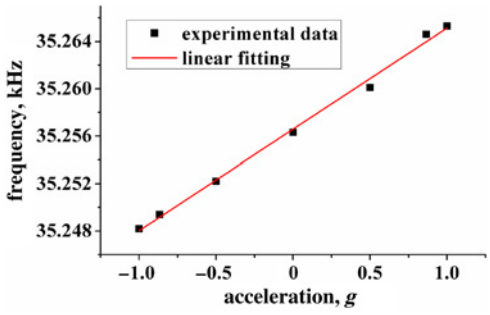

Figure 12 *Function of acceleration and sensor output*

the dividing head rotates from 0 to 180°, so the sensitivity is 8.55 Hz/*g*. The resonance frequency of the DETF is 35.2563 kHz when no acceleration is applied. The experiment results are in good agreement with the FE simulation. The FE simulated sensitivity and resonant frequency for no loading are 9.17 Hz/*g* and 34.581 kHz, respectively. The main reason that induced the error of the theoretical result (38.535 kHz) is that the quartz is regarded as an isotropic material for simplification.

The function relationship between acceleration and sensor output is established according to (2), and the results are presented in Figs. 12 and 13. The sensor nonlinearity can be calculated according to the data of Fig. 12 and it is 0.05% FS within ±1 *g*. Fig. 13 shows the loading process and the corresponding unloading process, and the hysteresis can be calculated, which is 0.003% FS.

To evaluate the effectiveness of the isolator, a similar sensor with exactly the same size and the DETF was designed and fabricated for comparison, as shown in Fig. 14.

The proof mass is also suspended by two suspension beams and the package of the sensor is also the same. The temperature coefficient of the offset (TCO) was measured within the temperature range from 0 to 50°C, as shown in Table 1.

Then, we compared the TCO value with that without the isolator and some references, as shown in Table 2. Experimental results

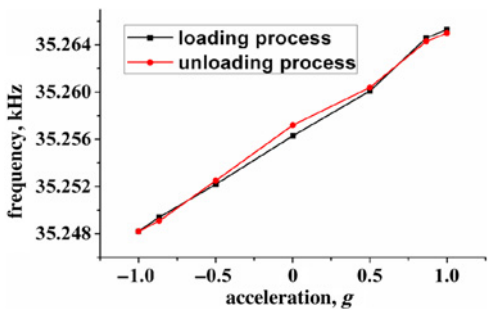

Figure 13 *Loading and unloading experimental results within ±1 g*

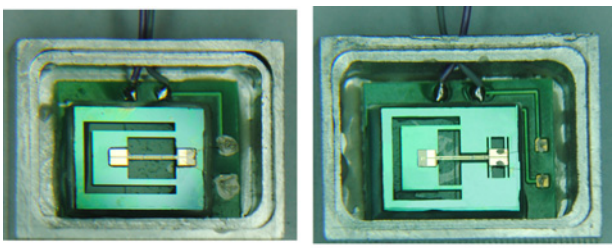

Figure 14 *Two different structures for validation of temperature isolator*
a Similar structure for comparison
b Proposed structure

Table 1 Experimental data of temperature influence

Temperature/°C	Output/kHz	TCO
0	35.6203	0.0006/°C
10	35.4054	
20	35.1736	
30	34.9415	
40	34.6931	
50	34.4036	

Table 2 Comparison of TCO values

	Without isolator	With isolator	Reference [14]	Reference [15]
TCO/°C	0.001	0.0006	0.000089	0.00229

show that the isolator is effective for decreasing the temperature influences. The TCO value for the structure with the isolator is at the average level.

More performances of the sensor were tested. The zero-point offset is no more than 0.5 Hz in 1 h, which is 0.0014% of the output average. The tumbling experiment was also carried out to measure the *X*-direction and *Y*-direction sensitivity, and the values are 0.7 and 0.8 Hz/*g*, respectively.

5. Conclusion: In this Letter, a resonant accelerometer, which is made up of silicon substrate and the DETF, is described, and it has been simulated and characterised. The analytic calculation shows that the isolator decreased thermal stress by 30.2%. The sensitivity, nonlinearity and hysteresis of the proposed sensor is 8.55 Hz/*g*, 0.05% FS and 0.003% FS, respectively. The TCO is 0.0006/°C within the temperature range from 0 to 50°C. The fluctuation of the zero-point frequency in 1 h is <0.5 Hz. The experimental results confirm the feasibility of the sensor configuration.

6. Acknowledgments: This work is supported by the National Nature Science Foundation for Distinguished Young Scholars (grant no. 51325503) and by the Changjiang scholars and Innovative Research Team in University of China (grant no. IRT1033).

7 References

[1] Albert W.C.: 'Vibrating quartz crystal beam accelerometer'. 28th Int. Instrumentation Symp., Las Vegas, NV, USA, 1982, pp. 33–44
[2] Langdon R.: 'Resonator sensors – a review', *J. Phys. E, Sci. Instrum.*, 1985, **18**, (2), pp. 103–115
[3] Stemme G.: 'Resonant silicon sensors', *J. Micromech. Microeng.*, 1991, **1**, pp. 113–125
[4] Olsson R.H., Wojciechowski K.E., Baker M.S., Tuck M.R., Fleming J.G.: 'Post-CMOS-compatible aluminum nitride resonant MEMS accelerometers', *J. Microelectromech. Syst.*, 2009, **18**, (3), pp. 671–678
[5] Kanda K., Nagata K., Yamakawa T., Iga Y., Fujita T., Maenaka K.: 'Miniaturization of vibratory beam accelerometer by using PZT', *Procedia Eng.*, 2012, **47**, pp. 1141–1144
[6] Satchell D., Greenwood J.: 'A thermally-excited silicon accelerometer', *Sens. Actuators*, 1989, **17**, pp. 241–245
[7] Chen D., Wu Z., Liu L., Shi X., Wang J.: 'An electromagnetically excited silicon nitride beam resonant accelerometer', *Sensors*, 2009, **9**, pp. 1330–1338
[8] Kass W.J., Snow G.S.: 'Double-ended tuning fork quartz accelerometer'. Proc. 40th Annual Frequency Control Symp., Philadelphia, PA, USA, 1986, pp. 230–236
[9] Norling B.L., Cornelius C.J.: 'Accelerometer with isolator for common mode inputs'. U.S. patent 4766768, 1988
[10] Le Traon O., Janiaud D., Lecorre B., Pernice M., Muller S., Tridera J. Y.: 'Monolithic differential vibrating beam accelerometer within an isolating system between the two resonators'. Proc. IEEE Int. Conf. on Sensors, Irvine, CA, USA, 2005, pp. 648–651
[11] Le Traon O., Janiaud D., Pernice M., Masson S., Muller S., Tridera J.: 'A new quartz monolithic differential vibrating beam accelerometer'. Proc. IEEE/ION Position Location and Navigation Symp. (PLANS), San Diego, CA, USA, 2006, pp. 6–15
[12] Bao M.: 'Analysis and design principles of MEMS devices' (Elsevier, 2005), p. 80
[13] Bouwstra S., Geijselaers B.: 'On the resonance frequencies of microbridge'. Dig. Tech. Pap. 6th Int. Conf. Solid-State Sensors and Actuators, San Francisco, CA, USA, 1991, pp. 538–542
[14] Wang J., Li X.: 'A high-performance dual-cantilever high-shock accelerometer single-sided micromachined in (111) silicon wafers', *J. Microelectromech. Syst.*, 2010, **19**, (6), pp. 1515–1520
[15] Liu Y., Zhao Y., Wang W., Sun L., Jiang Z.: 'A high-performance multi-beam microaccelerometer for vibration monitoring in intelligent manufacturing equipment', *Sens. Actuators A, Phys.*, 2013, **189**, pp. 8–16

doi: 10.1049/mnl.2014.0265